Acetylated Trifluoromethyl Diboronic Acid Anthracene with a Large Stokes Shift and Long Excitation Wavelength as a Glucose-Selective Probe

Hongsik Choi [†], Inhyeok Song [†], Chul Soon Park, Heung-seop Yim * and Joong Hyun Kim *

Drug Manufacturing Center, Daegu-Gyeongbuk Medical Innovation Foundation, 80 Chumbok-ro, Dong-gu, Daegu City 41061, Korea; hschoi@kmedihub.re.kr (H.C.); sih1222@kmedihub.re.kr (I.S.); cspark@kmedihub.re.kr (C.S.P.)
* Correspondence: yimhs@kmedihub.re.kr (H.-s.Y.); jhkim@kmedihub.re.kr (J.H.K.)
† These authors contributed equally to this work.

Featured Application: Glucose detection such as in-vivo continuous glucose monitoring or point-of-care detection.

Abstract: Continuous control of blood glucose levels is important for the effective treatment of diabetes. The short-term use of enzymatic continuous monitoring systems involves expensive maintenance and is inconvenient, which limits their widespread use by diabetes patients. The fluorescent diboronic anthracene-embedded system has demonstrated in vivo continuous glucose monitoring for 12 times longer than enzymatic systems by protecting the dye from reactive oxygen species. However, its small Stokes shift and low excitation and emission wavelength should be heavily considered for easy fabrication. We successfully synthesized a derivative of bis-phenyl boronate with a large Stokes shift and long excitation wavelength by adding an acetyl moiety to the anthracene ring. This resulted in a ~90-nm Stokes shift and 15-nm and 80-nm redshifts of the excitation and emission wavelengths, respectively. The fluorescence of the synthesized probe increased proportionally with the glucose concentration because the formation of the boronic acid-glucose complex prevented photoinduced electron transfer. The association constant and quantum yield for acetyl-substituted diboronic anthracene with glucose was 20% and 13% higher than that of the analog, respectively. While keeping resistance to the oxidation by reactive oxygen species, the improved optical properties and glucose-detecting performances of the newly synthesized dye will allow better pairing of the source and detecting unit for in vivo continuous glucose monitoring, leading to easy fabrication and then contributing more to utilization by diabetes patients.

Keywords: diboronic acids; stokes shift; photoinduced energy transfer; diabetes; glucose sensor

1. Introduction

Control of blood glucose levels is extremely important for patients with diabetes [1–4]. However, unpredictable fluctuations in blood glucose levels and variations between individual patients make it difficult to effectively treat diabetes [5,6]. Particularly, special care is required for insulin-dependent diabetes patients because insulin injection can sometimes result in hypoglycemia, leading to coma or death. Therefore, continuous glucose monitoring (CGM) is recommended for such patients. Four CGM systems are available on the market [7]. Most of these systems are enzyme-immobilized needle-injection systems. The high maintenance cost and inconvenience of replacing the sensors every 6–14 days is the main hurdle for their widespread use [8]. Globally, a very low percentage of patients with diabetes who require CGM use the systems worldwide [9]. While there have been great efforts to increase the instability of enzymes, the period of use of the enzymatic CGM systems has been not increased for a long time [10,11]. The one non-enzymatic CGM

system relies on a diboronic acid-based fluorescent molecule. For the specific and reversible interaction of diboronic acids with glucose, several derivatives have allowed in vivo glucose monitoring [12–17]. The immune response to the implanted device generates reactive oxygen species (ROS) such as H_2O_2 [18]. Therefore, resistance to ROS is highly important for the long-term use of CGM. The addition of an electron acceptor group to the aromatic moieties with boronate residues increased the resistance to oxidation by ROS [19]. For example, trifluoromethyl-substituted dibornic acid anthracene resulted in a 24-fold increase in the half-life for 10 μM of H_2O_2 [20]. Additionally, the fluorescent probe under the skin can be protected against reactive oxygen species (ROS) by a platinum coating. As the result, the non-enzymatic implantable system can be used for up to 180 days [13]. However, the excitation and emission spectrum of the dye are largely overlapped. The maximum excitation and emission wavelengths of the used trifluoromethyl derivative were approximately 405 nm and 430 nm, respectively. The largely overlapped spectra and the small Stokes shift make it difficult to select a light source and detector pair. To minimize the noise resulting from the overlapped spectra, the system needs to use a higher excitation energy source than the dye's maximum excitation and an additional photodiode as a reference, aside from the main one [21]. The lower excitation wavelength can result in more heat generation and energy consumption. Therefore, improvement of the optical characteristics, such as a large Stokes shift and longer excitation wavelength, is still in demand. In this study, we report the synthesis of a new diboronic anthracene with a larger Stokes shift and longer excitation wavelength than the commercially used analog. It is known that the acetyl group can increase the emission wavelength of the dye [22,23]. By introducing the acetyl group on the anthracene, we could increase the Stokes shift up to 90 nm. The introduced acetyl group did not affect the resistance to ROS. Instead, the acetylation resulted in an improved glucose detecting ability for the dye.

2. Materials and Methods

2.1. Materials

The 9,10-dimethylanthracene (98%) was purchased from Angel Pharmatech Ltd. (Shanghai, China). The β-alanine t-butyl ester hydrochloride, n-(3-aminopropyl) methacrylamide hydrochloride (97%) was purchased from Leap Labchem Co. (Hong Kong, China). Other starting materials for the synthesis and solvents were purchased from Aldrich, TCI, and Alfa Aesar and used without further purification. Fluorescein, D-(+) galactose (≥98%), D-mannitol (≥98%), D-(+) maltose (≥99%), sucrose (≥99.5%), and ibuprofen (≥98%) were purchased from Sigma-Aldrich (St. Louis, MO, USA). D-glucose (≥98%), D-fructose (≥99%), and lactose were purchased from Junsei (Saitama, Japan). Dimethyl sulfoxide (≥99%) was purchased from Duksan (Gyeonggi-do, Korea). Sodium hydroxide (≥97%) was purchased from Daejung (Gyeonggi-do, Korea). PBS (10X) was purchased from GenDEPOT (Katy, TX, USA).

2.2. Methods

2.2.1. Measurement of Saccharide-Dependent Fluorescence

Stock solutions were prepared by dissolving 40-mM dyes in DMSO and storing them at 4 °C before use. The stock solution was diluted in 1× PBS (pH 7.4) to obtain 20 μM of the dye in the buffer. The dye solution was mixed with an equal volume of the saccharide solution. The saccharide mixture (200 μL) was transferred to a black 96-well plate (SPL Life Science Co., Ltd., Pocheon-si, Korea), and the fluorescence was measured using a SpectraMaxiD3 (Molecular Devices, San Jose, CA, USA).

2.2.2. Measurement of Decay Time

The dye (20 μM) in the buffer containing 200 mg/dL glucose was prepared from the stock solution. The time-resolved fluorescence intensity at 490 nm of the mixture (200 μL) in the 96-well plate was measured every 30 s after adding 10 mM H_2O_2 to the mixture using the well plate reader.

2.2.3. Relative Quantum Yield

The emission spectra of AcTDA and TDA in SpectraMaxiD3 1× PBS were recorded. For the relative quantum yield, the emission spectra of fluorescein at the various concentrations in 0.1 M NaOH were also measured at 360 nm and 340 nm of excitation for AcTDA and TDA, respectively. The area of the emission spectra of each dye at the measured concentrations (1 μM, 5μM, 10 μM, and 20 μM) were plotted with the corresponding absorbance at 360 nm and 340 nm for AcTDA and TDA, respectively.

3. Results

3.1. Synthesis

The acetylated diboronic anthracenes were prepared according to the synthetic routes shown in Scheme 1. The detailed synthetic procedure is described below.
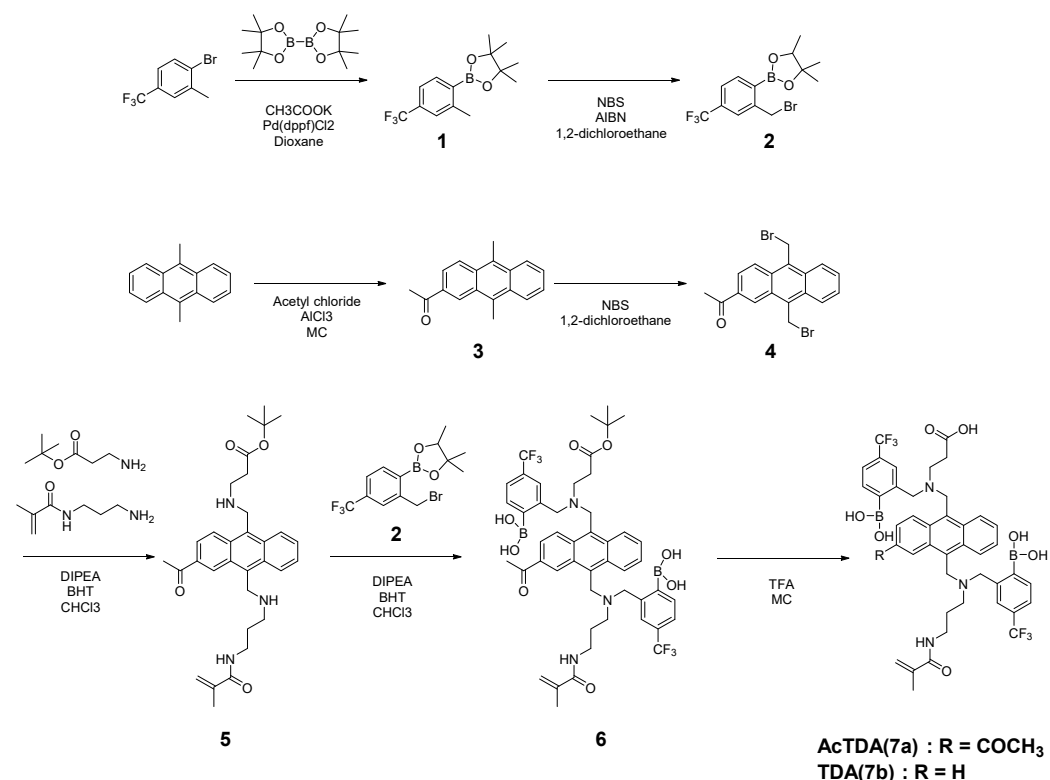
Scheme 1. Synthesis route of acetylated trifluoromethyl diboronic anthracene (AcTDA).

3.1.1. 4,4,5,5-Tetramethyl-2-(2-methyl-4-(trifluoromethyl)phenyl)-1,3,2-dioxoborolane (Compound **1**)

Compounds of 1-bromo-2-methyl-4-(trifluoromethyl) benzene (20.00 g, 0.084 mol), 4,4,4′,4′,5,5,5′,5′-octamethyl-2,2′-bis(1,3,2-dioxoborolane) (42.5 g, 0.167 mol), potassium acetate (32.85 g, 0.335 mol), and [1,1′bis(diphenylphosphino)ferrocene]dichloropalladium(II) (6.12 g, 0.0084 mol) in 600 mL of dioxane were stirred at 100 °C for 1 h. After the solution was cooled to room temperature, 600 mL of DI water was added into the mixture, and the mixture was extracted using methylene chloride (600 mL). The organic layer of the mixture was separated and dried over anhydrous magnesium sulfate. The dried compound was stirred in 500 mL of hexane for 0.5 h until the formation of precipitation. Oily compound **1** (21.5 g, 89.9%) was obtained after the formed precipitate was filtered off and purified using silica gel chromatography with dichloromethane/hexane (1:8, *v/v*) as the eluent (^{1}H NMR (400 MHz, chloroform-d): δ 7.88(d, 1H), 7.43–7.41(m, 2H), 2.61(s, 3H), and 1.38(s, 12H)).

3.1.2. 2-(2-(Bromomethyl)-4-(trifluoromethyl)phenyl)-4,4,5,5-tetramethyl-1,3,2-dioxoborolane (Compound **2**)

4,4,5,5-tetramethyl-2-(2-methyl-4-(trifluoromethyl)phenyl)-1,3,2-dioxoborolane (21.5 g, 0.075 mol) and N-bromosuccinimide (NBS) (14.7 g, 0.083 mol) were dissolved in 390 mL of 1,2-dichloroethane, and 2,2-azobisisobutyronitrile (AIBN) (1.23 g, 0.075 mol) was added into the mixture and stirred at 80 °C for 3 h before the mixture was allowed to cool to RT, followed by filtration. After removal of the solvent under reduced pressure, the mixture was stirred in 200 mL of hexane for 0.5 h. Yellow oily compound **2** was obtained after evaporating the solvent of the filtered-off precipitate under a vacuum (yield (29.00 g, 10.6%); ^{1}H NMR (400 MHz, chloroform-d): δ 7.93(d, 1H), 7.63(s, 1H), 7.52(d, 1H), 4.92(s, 2H), and 1.39(s, 12H)).

3.1.3. 2-Acetyl-9,10-dimethylanthracene (Compound **3**)

9,10-dimethylanthracene (20.0 g, 0.1 mol) was dissolved in methylene chloride (600 mL). Acetyl chloride (0.4 g, 0.12 mol) and 18.8 g (0.149 mol) of aluminum chloride were added into the mixture and stirred at 0~5 °C. After 5 h of additional stirring at RT and refluxing for 1 h, the mixture was allowed to cool to RT. Then, 1 kg of ice and 50 mL of hydrochloric acid were added into the reaction mixture. The mixture was extracted with methylene chloride and water. After removal of the solvent under reduced pressure, the product was purified using silica gel chromatography with ethyl acetate/hexane (1:10, *v/v*) as the eluent. Compound **3** was obtained as a yellow powder in 56.5% yield (14.0 g); ^{1}H NMR (400 MHz, chloroform-d): δ 9.00(m, 7H), 3.15(d, 6H), and 2.80(s, 3H).

3.1.4. 2-Acetyl-9,10-bis(bromomethyl)anthracene (Compound **4**)

2-acetyl-9,10-dimethylanthracene (14.0 g, 0.056 mol) was dissolved in 1,2-dichloroethane (300 mL). After the complete addition of N-bromosuccinimide (22.1 g, 0.124 mol), the reaction solution was stirred for 1 h at 85 °C. The reaction mixture was allowed to cool to RT, and the solvent was evaporated under reduced pressure. After the mixture was stirred in 150 mL of methanol for 0.5 h, the precipitate was filtered, washed with methanol, and dried under a vacuum at 40 °C for 12 h. The obtained compound (compound **4**) was a bright yellow powder (yield: 7.7 g, 33.6%; ^{1}H NMR (400 MHz, chloroform-d): δ 9.00–7.50(m, 7H), 5.50(d, 4H), and 2.80(s, 3H)).

3.1.5. Tert-butyl 3-(([3-acetyl-10-(([3-methacrylamidopropyl]amino)methyl)anthracen-9-yl]methyl)amino)propanoate (Compound **5**)

Compound **4** (7.7 g, 0.019 mol) consisted of β-alanine t-butyl ester hydrochloride (12.5 g, 0.069 mol), n-(3-aminopropyl) methacrylamide hydrochloride (12.3 g, 0.069 mol), butylated hydroxytoluene (BHT) (0.28 g, 0.00127 mol), and NN-diisopropylethylamine (DIPEA) (24 mL, 0.138 mol) in 400 mL of chloroform dissolved at 30 °C for 18 h. After the solvent was evaporated under reduced pressure, the mixture was washed with distilled water (3 times × 200 mL) and dried over $MgSO_4$. The obtained crude product was purified using silica chromatography with $CHCl_3$/MeOH (95:5, *v/v*) with the eluent. A yellow powder was obtained (yield: 1.1 g, 15.0%; ^{1}H NMR (400 MHz, chloroform-d): δ 8.70–7.29(m, 8H), 5.79(s, 1H), 5.72(s, 1H), 4.16(m, 6H), 3.18(d, 2H), 2.94(d, 2H), 2.50(m, 7H), 1.98(s, 3H), 1.74(t, 2H), and 1.42(s, 9H); LC-MS: calculated for $C_{32}H_{41}N_3O_4$ *m/z*, 531.70; found *m/z*: 532 [M + H]+).

3.1.6. (2-([(((3-Acetyl-10-[((2-borono-5-[trifluoromethyl]benzyl)[3-methacrylamidopropyl]amino)methyl)anthracen-9-yl]methyl)(3-[tert-butoxy]-3-oxopropyl)amino)methyl]-4-(trifluoromethyl)phenyl)boronic Acid (Compound **6**)

Compound **5** (0.2 g, 0.38 mmol) and NN-diisopropylethylamine (DIPEA) (520 mL, 2.97 mmol) in 20 mL of chloroform were stirred at RT. Butylated hydroxytoluene (BHT) (0.01 g, 0.038 mmol), 2-(2-(bromomethyl)-4-(trifluoromethyl) phenyl)-4,4,5,5-tetramethyl-1, and 3,2-dioxoborolane (0.535 g, 1.47 mmol) were added into the reaction mixture, followed by stirring at RT for at least 24 h. After removal of the solvent-reduced pressure, the mixture

was dissolved in 20 mL of isopropyl ether and washed 3 times with 20 mL of phosphate buffer (0.2 M, pH 7.0). After removal of the solvent, the product was purified using silica gel chromatography, with $CHCl_3$/MeOH (98:2, *v*/*v*) as the eluent. A yellow powder was obtained in a 48.3% yield (0.2 g) (^{1}H NMR (400 MHz, chloroform-*d*): δ 8.70–7.28(m, 14H), 5.79(s, 1H), 4.20(s, 4H), 4.10(s, 2H), 3.76–3.66(m, 6H), 3.18(d, 2H), 2.46(m, 7H), 1.98(s, 3H), 1.73(t, 2H), and 1.42(s, 9H); LC-MS: calculated for $C_{48}H_{53}B_2F_6N_3O_8$ *m*/*z*: 935.58; found *m*/*z*: 936 [M + H]+; 918 [M-H_2O + H]$^+$ and 900 [M-2H_2O + H]$^+$).

3.1.7. 3-(((3-Acetyl-10-(((2-borono-5-(trifluoromethyl)benzyl)(3-methacrylamidopropyl) amino)methyl)anthracen-9-yl)methyl)(2-borono-5-(trifluoromethyl)benzyl)amino) propanoic Acid (Compound **7a**)

Compound **6** (0.2 g, 0.182 mmol) in 5 mL of methylene chloride containing 20 wt% trifluoroacetic acid was stirred at room temperature for 20 h. After evaporating the solvent under a vacuum, the product was purified using silica gel chromatography with $CHCl_3$/MeOH (95:5, *v*/*v*) as the eluent. A yellow powder was obtained in a 43.5% yield (0.074 g) (^{1}H NMR (400 MHz, chloroform-d): δ 12.27(s, 1H), 8.70–7.28 (m, 14H), 5.79(s, 1H), 4.20(s, 4H), 4.10(s, 2H), 3.76–3.66(m, 6H), 3.18(d, 2H), 2.46(m, 7H), 1.98(s, 3H), 1.73(t, 2H), and 1.42(s, 9H); LC-MS: calculated for $C_{44}H_{45}B_2F_6N_3O_8$ *m*/*z*: 879.47; found *m*/*z*: 880 [M + H]+; 862 [M-H_2O + H]$^+$, 844[M-2H_2O + H]$^+$).

3.1.8. 3-((2-Borono-5-(trifluoromethyl)benzyl)((10-(((2-borono-5-(trifluoromethyl)benzyl) (3-methacrylamidopropyl)amino)methyl)anthracen-9-yl)methyl)amino)propanoic acid (Compound **7b**)

After carrying out the same procedure, compound **7b** was synthesized through the same steps except for acetylation. A yellow powder was obtained in a 51.2% yield (0.089g) (^{1}H NMR (400 MHz, chloroform-*d*): δ 8.28–7.38(m, 14H), 5.35(s, 1H), 5.05(s, 1H), 4.95(t, 1H), 4.55(s, 2H), 4.44(s, 2H), 4.35(s, 2H), 4.05(s, 2H), 2.92(m, 2H), 2.87(m, 2H), 2.44(t, 2H), 2.31(t, 2H), 1,58–1.60(m, 5H), 1.38(s, 12H), and 1.34(s, 12H); LC-MS: calculated for $C_{42}H_{43}B_2F_6N_3O_7$ *m*/*z*: 837.43; found *m*/*z*: 838 [M + H]+; 820 [M-H_2O + H]$^+$, 802[M-2H_2O + H]$^+$).

3.2. Fluorogenic Optical Properties

After synthesizing acetylated trifluoromethyl diboronic anthracenes (AcTDAs) and trifluoromethyl diboronic anthracenes (TDAs), we characterized the optical properties of the analogs by measuring and comparing the emission and excitation spectra. Figure 1 shows the spectra for both molecules. AcTDA, which has trifluoromethyl and acetyl groups, exhibited excitation and emission wavelengths at 420 nm and 510 nm, respectively (Figure 1a). In contrast, TDA, the counter-diboronic anthracene with no acetyl group, demonstrated the longest excitation and emission wavelengths at 405 nm and 430 nm, respectively. These results clearly demonstrated that the addition of an acetyl group resulted in ~80 nm and 15 nm red-shifted maximum emission and excitation wavelengths, respectively. Table 1 shows the excitation and emission wavelengths of the reported diboronic anthracene derivatives. As shown in Table 1, diboronic anthracene with an acetyl group on the anthracene produced a relatively large Stokes shift with a long excitation wavelength. This analysis confirms the increase in the Stokes shift and excitation wavelength by the acetyl group on the anthracene. Among the diboronic anthracene derivatives reported in Table 1, AcTDA exhibited the largest Stokes shift with the longest excitation wavelength [14,23–26]. Compared with similar acetylated derivatives [23], AcTDA produced excitation and emission fluorescence that was red-shifted by at least 15 and 22 nm, respectively. It has been reported that the substitution of a trifluoromethyl group on the quinoline ring of thiazole orange led to a redshift of thiazole orange [27]. Therefore, the two electron-withdrawing groups resulted in the largest Stokes shift with the longest excitation and emission wavelengths.
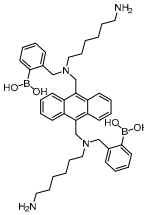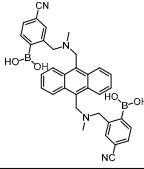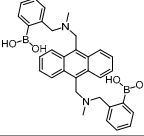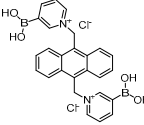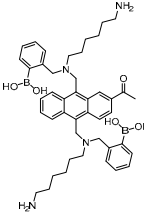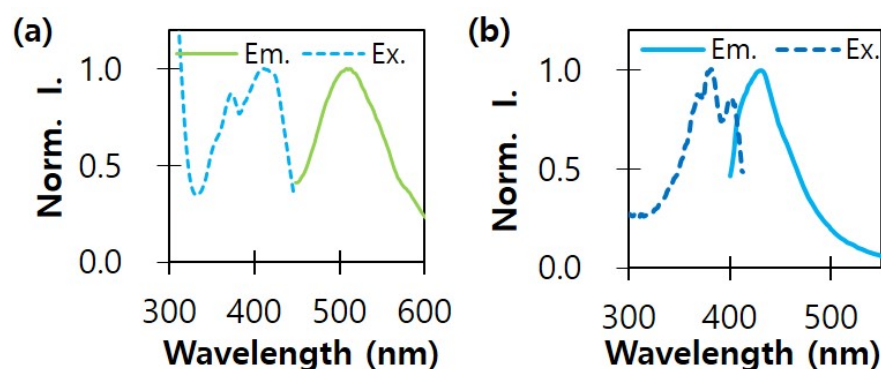
Figure 1. Emission (Em.) and excitation (Ex.) spectra of trifluoromethyl diboronic anthracenes (**a**) with and (**b**) without an acetyl group. Norm. I. denotes normalized emission and excitation intensity at the maximum wavelength.

Table 1. Emission and excitation wavelength of the reported derivate of diboronic acid anthracene.

Structure	λ_{ex} (nm)	λ_{em} (nm)	Ref.
	400	480	[24]
	375	405/427	[25]
	370	423	[14]
	377	427	[26]
	405	488	[23]

3.3. Measurement of Oxidation Resistance

For the long-term operation of the implanted CGM system, resistance to ROS is extremely important. As mentioned previously, trifluoromethyl substitution increased the resistance to oxidation of the hydroxyl groups of boronate, which interacted with the diol of glucose to form a boronic acid-glucose complex. To determine how the added acetyl group affected the resistance, we measured the changes in the fluorescence intensity of the two analogs in the presence of hydrogen peroxide, the main ROS generated by the immune response to the implanted device [20,28–30]. As shown in Figure 2, the two

analogs exhibited identical decay rates of fluorescence intensity. This result indicates that the substituted acetyl group did not affect the oxidation resistance.
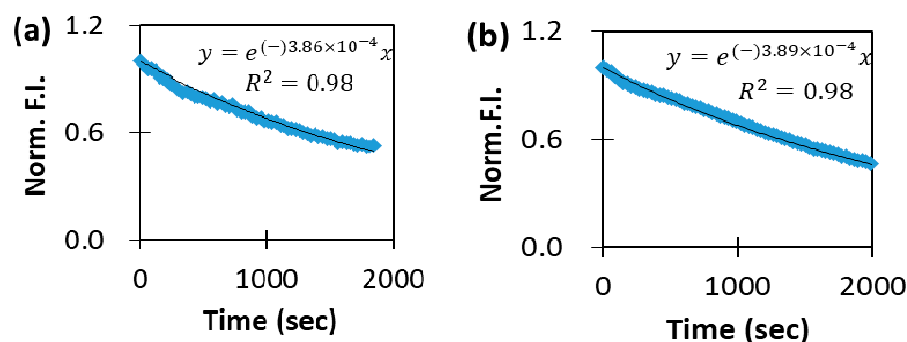

Figure 2. Comparison of oxidation resistance of AcTDA and TDA. Normalized fluorescence intensity after 4 mM H_2O_2 was added to 20 µM of (**a**) AcTDA and (**b**) TDA with 200 mg/dL glucose in 1× PBS (pH 7.4).

3.4. Glucose-Dependent Optical Characterisitcs

Next, we explored the fluorescence change of AcTDA with changes in the glucose concentration by collecting the emission spectra of the compound with various concentrations of glucose. Figure 3 shows the measured emission spectra of AcTDA mixed with glucose. In the presence of glucose, the emission spectra were blue-shifted by ~20 nm, and the intensity increased. According to the mechanism of B-N bond formation, the formation of a boronic acid complex with the diols from a saccharide, such as glucose, created intramolecular interactions between the boronic acids and amines. As shown in Figure 4, the B-N bond prevented the nitrogen lone pair from participating in photoinduced electron transfer (PET) [14,31]. As a result, the quenched anthracene fluorescence was recovered. Thus, we could observe the increased fluorescence intensity of AcTDA as the glucose level of the mixture increased. Next, we measured the association constant of AcTDA with glucose using the modified Benesi–Hildebrand plot [25]:

$$\frac{1}{F - F_0} = \frac{1}{Ka \times (F_{max} - F_0) \times [Glucose]} + \frac{1}{F_{max} - F_0} \tag{1}$$

where F is the measured fluorescence intensity, F_0 is the fluorescence intensity of free AcTDA, and F_{max} is the saturated fluorescence intensity of the AcTDA–glucose complex. We plotted $1/[F - F_0]$ versus $1/[glucose]$ and calculated the association constant for the obtained linear relationship (Figure 3d). The obtained association constant with glucose was 730 ± 18 M^{-1}. We also measured the association constant of TDA with glucose. Figure 5 shows the fluorescence changes for TDA, depending on the quantity of added glucose. As shown in Figure 5, the fluorescence intensity of TDA increased proportionally with an increasing glucose concentration. The calculated association constant was 606 ± 63 M^{-1}, which was approximately 20% lower than that of AcTDA. As shown in Figure 5c, no significant spectral shift was observed for glucose mixed with TDA. Instead, the emission peak became narrower. Because the portion of fluorescence from the unbound AcTDA that contributed to the association calculation was smaller than that of TDA, AcTDA could have a higher binding affinity for glucose than TDA. Meanwhile, there was no shift in the excitation spectrum of either dye by glucose (Figure S1). The excitation intensity near 300 nm was decreased for both dyes in the presence of glucose because the contribution of the plastic well plate to the excitation decreased. In addition, we compared the quantum yield of the two analogs by measuring the relative quantum yield [32]. The relative quantum yield is calculated using a flowing equation:

$$Q_S = Q_R \left(\frac{m_r}{m_s} \right) \left(\frac{n_s}{n_r} \right)^2 \tag{2}$$

where Q is the quantum yield, m is a gradient of the plot of the integrated fluorescence against absorbance, n is the refractive index of the solvent, and s and r are the sample and reference, respectively. In the equation, the quantum yield of reference is independent of the excited wavelength, but the ratio of the plot of integrated fluorescence against the absorbance is a function of the exciting wavelength [30]. Then, Equation (2) can be rearranged to the ratio of the quantum yield between two samples as follows:

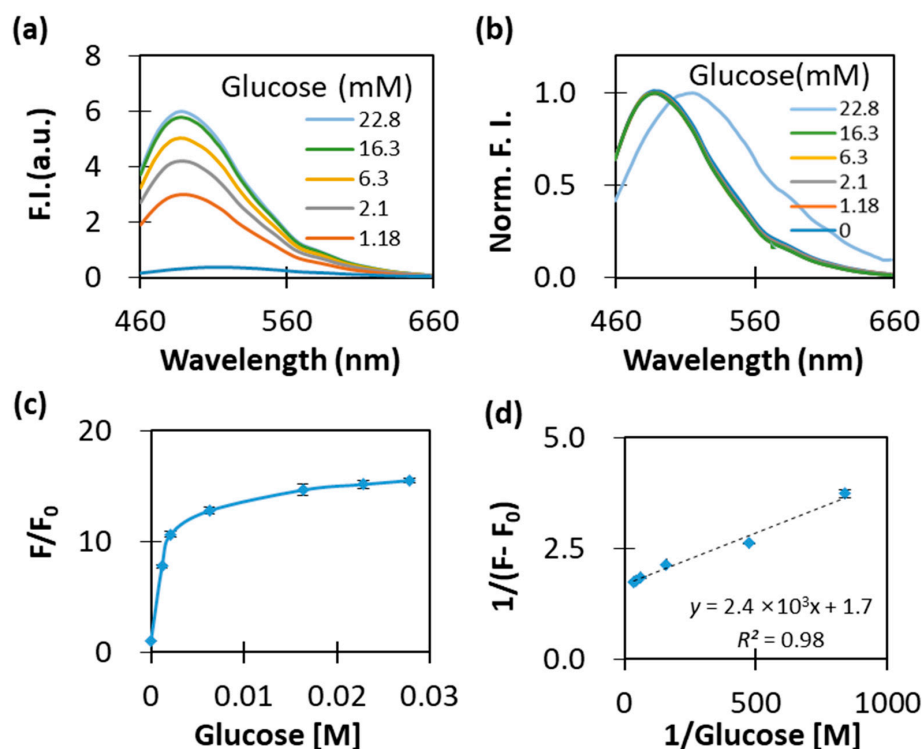$$\frac{Q_{S1}}{Q_{S2}} = \left(\frac{m_{r1}}{m_{s1}}\right)\left(\frac{m_{r2}}{m_{s2}}\right) \tag{3}$$

Figure 3. Glucose binding properties of AcTDA. (**a**) Emission spectra and (**b**) normalized emission spectra for glucose at concentrations of 0–500 mg/dL. Fluorescence intensity at the maximum wavelength was used for the normalization. (**c**) Relative fluorescence intensity. (**d**) Benesi–Hildebrand plot.
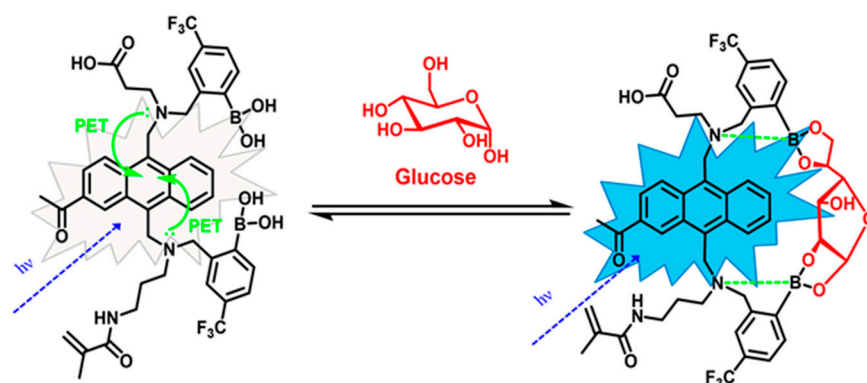

Figure 4. Glucose-dependent fluorescence change for AcTDA. Quenched fluorescence of AcTDA was recovered after formation of AcTDA–glucose because photoinduced electron transfer was blocked by the B-N bond pair.
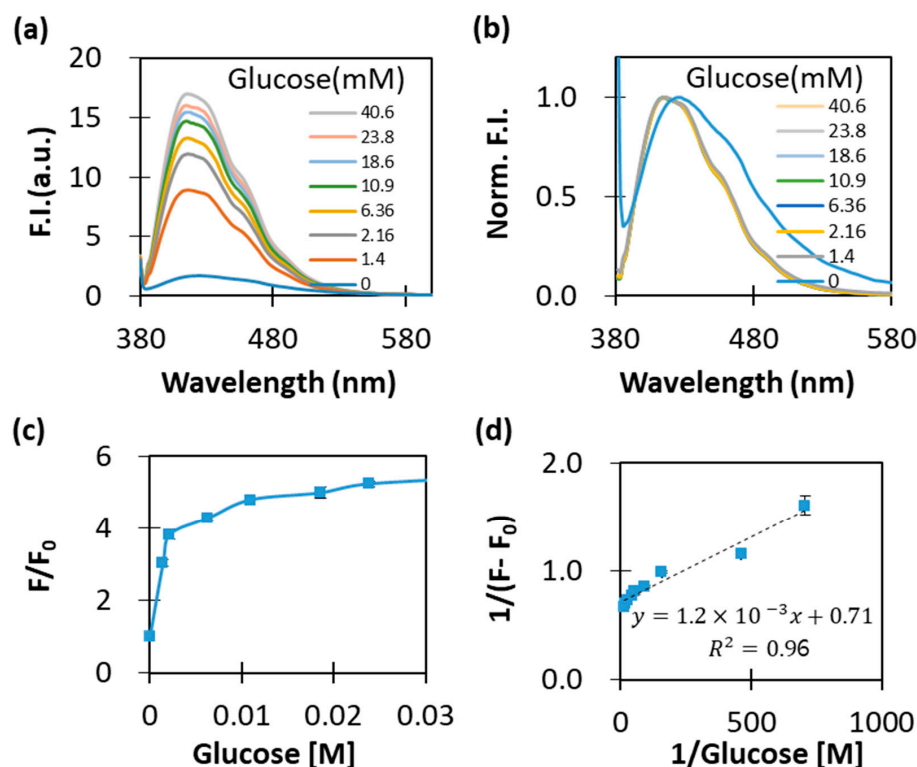
Figure 5. Glucose-binding properties of TDA. (**a**) Emission spectra. (**b**) Normalized emission spectra. Fluorescence intensity at the maximum wavelength was used for the normalization. (**c**) Relative fluorescence intensity. (**d**) Benesi–Hildebrand plot.

Using fluorescein as the reference, we obtained the gradient of each compound in the presence of 30 mM of glucose (Figure 6). According to Equation (3), the glucose-responding quantum yield of AcTDA was about 13% higher than that of TDA. In addition to the increased glucose binding affinity, the introduced acetyl group enhanced glucose responding quantum yield.
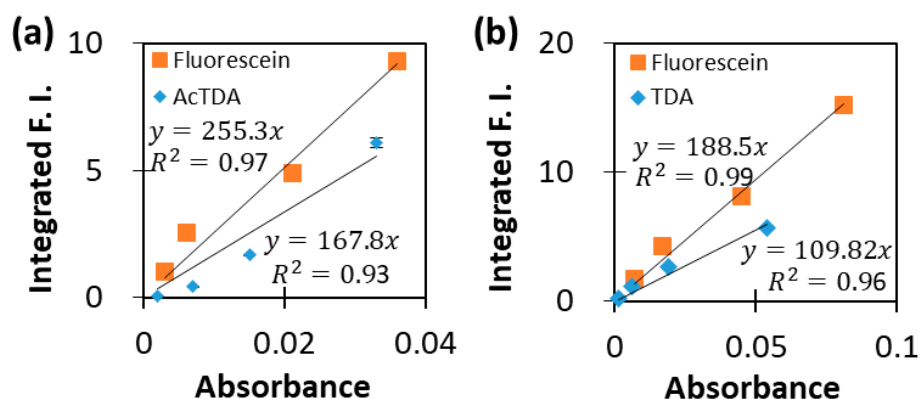

Figure 6. Gradient plot of integrated fluorescence intensity against absorbance for (**a**) AcTDA and fluorescein and (**b**) TDA and fluorescein.

3.5. Interference-Dependent Fluorescence

To use AcTDA as a glucose probe, it needs to demonstrate high specificity for glucose over other interferences, such as six-carbon sugars and common drugs. Therefore, we measured the fluorescence changes of AcTDA with six different saccharides, including fructose, galactose, lactose, maltose, mannitol, and sucrose, and the most common drugs.

For the drug ibuprofen, AcTDA did not show a meaningful fluorescence increase in the presence of maltose, sucrose, lactose, or ibuprofen (data not shown). Figure 7 shows

that the fluorescence increased when AcTDA was in the presence of fructose, galactose, and mannitol. The association constants for fructose and galactose were determined using the modified Benesi–Hildebrand plots (Figure S2). However, the modified Benesi–Hildebrand plot for AcTDA and mannitol did not exhibit a good fit (Figure S2). Therefore, we derived a plot to fit the fluorescence changes in response to mannitol (Figure S3) and obtained $213 \pm 4.5 \, \text{M}^{-1}$ as the association constant. The association constants decreased in magnitude in the following order: mannitol ($213 \pm 4.5 \, \text{M}^{-1}$) > fructose ($164 \pm 3.1 \, \text{M}^{-1}$) > galactose ($55 \pm 6.1 \, \text{M}^{-1}$). The association constant for glucose was at least 3.6-fold higher than those of the interfering saccharides. As the blood interference level (<0.1 mM) is much lower than that of glucose (3.6−5.8 mM), the quantity of glucose-bound AcTDA would be 123-fold higher than that of the interference-bound AcTDA [31]. Therefore, the interference could be considered negligible.
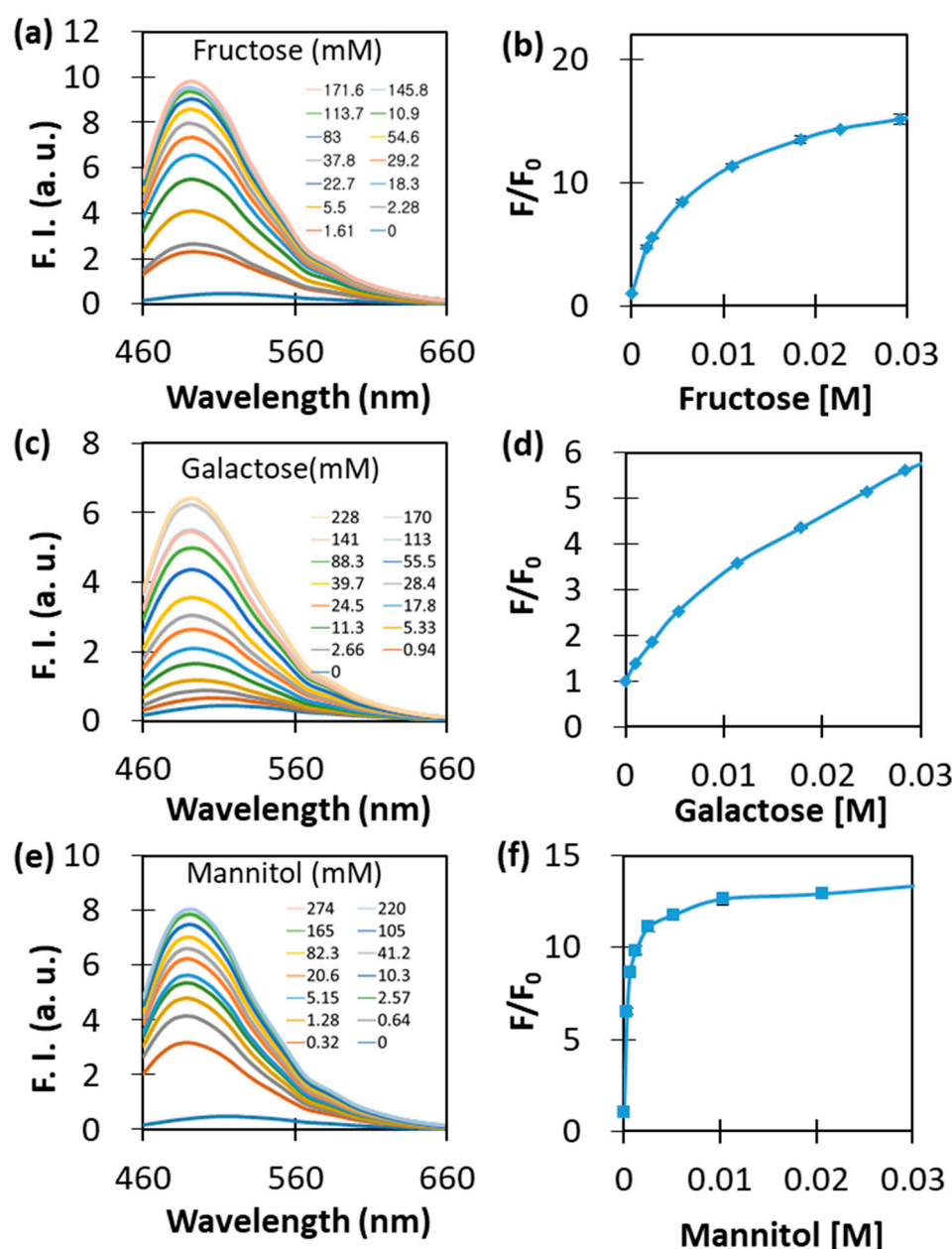

Figure 7. Binding properties of AcTDA with interferences. (**a**,**c**,**e**) Emission spectra for AcTDA with fructose, galactose, and mannitol, respectively. (**b**,**d**,**f**) Relative fluorescence intensity with fructose, galactose, and mannitol, respectively.

4. Conclusions

In conclusion, we successfully synthesized an oxidation resistant bis-phenyl boronate derivative with a large Stokes shift and long excitation and emission wavelengths by adding an acetyl moiety to the anthracene ring. The Stokes shift was the largest among the reported diboronic anthracene dyes. Moreover, the excitation wavelength was 420 nm, which was the longest of the reported diboronic anthracene dyes. The large Stokes shift and long excitation wavelength would allow the easy selection of an excitation-detecting unit and in vivo glucose monitoring. Moreover, the acetylated diboronic acid anthracene demonstrated good binding affinity and selectivity for glucose and an identical resistance to oxidation compared to the non-acetylated analog. The improved optical and glucose-detecting properties of the newly synthesized acetylated trifluoromethyl diboronic anthracenes can allow easy fabrication and reduce the power consumption of the system. Therefore, we expect that the reported dye in this work will be utilized to develop an affordable and long-term usable implantable CGM system for widespread use.

Supplementary Materials: The followings are available online at https://www.mdpi.com/article/10.3390/app12062782/s1. Figure S1: Excitation spectra in the presence of glucose for AcTDA (a) and TDA (b). Figure S2: The modified Benesi–Hildebrand plots of AcTDA with fructose (a), galactose (b), and mannitol (c), Figure S3: Association constant of AcTDA for mannitol.

Author Contributions: H.C. designed and synthesized the dyes; I.S. and J.H.K. carried out the characterization of the dyes; C.S.P. worked on the data presentation; H.-s.Y. and J.H.K. conceived these studies. All authors have read and agreed to the published version of the manuscript.

Institutional Review Board Statement: Not applicable.

Informed Consent Statement: Not applicable.

Conflicts of Interest: The authors declare no conflict of interest. The funders had no role in the design of the study; in the collection, analyses, or interpretation of data; in the writing of the manuscript, or in the decision to publish the results.

References

1. Koya, D.; King, G.L. Protein kinase C activation and the development of diabetic complications. *Diabetes* **1998**, *47*, 859–866. [CrossRef]
2. Brownlee, M. Biochemistry and molecular cell biology of diabetic complications. *Nature* **2001**, *414*, 813–820. [CrossRef] [PubMed]
3. Lee, T.H.; Marcantonio, E.R.; Mangione, C.M.; Thomas, E.J.; Polanczyk, C.A.; Cook, E.F.; Sugarbaker, D.J.; Donaldson, M.C.; Poss, R.; Ho, K.L.L.; et al. Derivation and prospective validation of a simple index for prediction of cardiac risk of major noncardiac surgery. *Circulation* **1999**, *100*, 1043–1049. [CrossRef] [PubMed]
4. Nestler, E.J.; Barrot, M.; DiLeone, R.J.; Eisch, A.J.; Gold, S.J.; Monteggia, L.M. Neurobiology of depression. *Neuron* **2007**, *34*, 13–25. [CrossRef]
5. Farmer, A.; Wade, A.; Goyder, E.; Yudkin, P.; French, D.; Craven, A.; Holman, R.; Kinmonth, A.-L.; Neil, A. Impact of self monitoring of blood glucose in the management of patients with non-insulin treated diabetes: Open parallel group randomised trial. *BMJ* **2007**, *335*, 132–139. [CrossRef] [PubMed]
6. Ginsberg, B.H. The current environment of CGM technologies. *J. Diabetes Sci. Technol.* **2007**, *1*, 117–121. [CrossRef] [PubMed]
7. Cappon, G.; Vettoretti, M.; Sparacino, G.; Facchinetti, A. Continuous glucose monitoring sensors for diabetes management: A review of technologies and applications. *Diabetes Metab. J.* **2019**, *43*, 383–397. [CrossRef] [PubMed]
8. Funtanilla, V.D.; Candidate, P.; Caliendo, T.; Hilas, O. Continuous glucose monitoring: A review of available systems. *Pharm. Ther.* **2019**, *44*, 550–553.
9. Petrie, J.R.; Peters, A.L.; Bergenstal, R.M.; Holl, R.W.; Fleming, G.A.; Heinemann, L. Improving the clinical value and utility of CGM systems: Issues and recommendations. *Diabetologia* **2017**, *60*, 2319–2328. [CrossRef]
10. Mano, N. Engineering glucose oxidase for bioelectrochemical applications. *Bioelectrochemistry* **2019**, *128*, 218–240. [CrossRef]
11. Beaufils, C.; Man, H.; Poulpiquet, A.; Mazurenko, I.; Lojou, E. From enzyme stability to enzymatic bioelectrode stabilization processes. *Catalysts* **2021**, *11*, 497. [CrossRef]
12. Joseph, J.I. Review of the long-term implantable senseonics continuous glucose monitoring system and other continuous glucose monitoring systems. *J. Diabetes Sci. Technol.* **2021**, *15*, 167–173. [CrossRef] [PubMed]

13. Colvin, A.E.; Jiang, H. Increased in vivo stability and functional lifetime of an implantable glucose sensor through platinum catalysis. *J. Biomed. Mater. Res. Part A* **2013**, *101*, 1274–1282. [CrossRef] [PubMed]

14. James, T.D.; Samankumara Sandanayake, K.R.A.; Iguchi, R.; Shinkai, S. Novel saccharide-photoinduced electron transfer sensors based on the interaction of boronic acid and amine. *J. Am. Chem. Soc.* **1995**, *117*, 8982–8987. [CrossRef]

15. Heo, Y.J.; Shibata, H.; Okitsu, T.; Kawanishi, T.; Takeuchi, S. Long-term in vivo glucose monitoring using fluorescent hydrogel fibers. *Proc. Natl. Acad. Sci. USA* **2011**, *108*, 13399–13403. [CrossRef]

16. Fang, G.; Wang, H.; Bian, Z.; Sun, J.; Liu, A.; Fang, H.; Liu, B.; Yao, Q.; Wu, Z. Recent development of boronic acid-based fluorescent sensors. *RSC Adv.* **2018**, *8*, 29400–29427. [CrossRef]

17. Wang, B.; Chou, K.H.; Queenan, B.N.; Pennathur, S.; Bazan, G.C. Molecular design of a new diboronic acid for the electrohydro-dynamic monitoring of glucose. *Angew. Chem. Int. Ed. Engl.* **2019**, *58*, 10612–10615. [CrossRef]

18. Li, W.; Sun, W.; Zhang, Y.; Wei, W.; Ambasudhan, R.; Xia, P.; Talantova, M.; Lin, T.; Kim, J.; Wang, X.; et al. Rapid induction and long-term self-renewal of primitive neural precursors from human embryonic stem cells by small molecule inhibitors. *Proc. Natl. Acad. Sci. USA* **2011**, *108*, 8299–8304. [CrossRef]

19. Yang, K.A.; Barbu, M.; Halim, M.; Pallavi, P.; Kim, B.; Kolpashchikov, D.M.; Pecic, S.; Taylor, S.; Worgall, T.S.; Stojanovic, M.N. Recognition and sensing of low-epitope targets via ternary complexes with oligonucleotides and synthetic receptors. *Nat. Chem.* **2014**, *6*, 1003–1008. [CrossRef]

20. Colvin, A.E., Jr.; Mortellaro, M.A.; Modzelewska, A. Oxidation Resistance Indicator Molecules. U.S. Patent No. 7,851,225 B2, March 2010.

21. DeHennis, A.; Getzlaff, S.; Grice, D.; Mailand, M. An NFC-Enabled CMOS IC for a wireless fully implantable glucose Sensor. *IEEE J. Biomed. Health Inform.* **2015**, *20*, 18–28. [CrossRef]

22. Diana, R.; Caruso, U.; Di Costanzo, L.; Bakayoko, G.; Panunzi, B. A novel DR/NIR T-shaped AIEgen: Synthesis and X-ray crystal structure study. *Crystals* **2020**, *10*, 269. [CrossRef]

23. Kawanishi, T.; Romey, M.A.; Zhu, P.C.; Holody, M.Z.; Shinkai, S. A study of boronic acid based fluorescent glucose sensors. *J. Fluoresc.* **2004**, *14*, 499–512. [CrossRef] [PubMed]

24. Shibata, H.; Heo, Y.J.; Okitsu, T.; Matsunaga, Y.; Kawanishi, T.; Takeuchi, S. Injectable hydrogel microbeads for fluorescence-based in vivo continuous glucose monitoring. *Proc. Natl. Acad. Sci. USA* **2010**, *107*, 17894–17898. [CrossRef] [PubMed]

25. Wang, K.; Zhang, R.; Yue, X.; Zhou, Z.; Bai, L.; Tong, Y.; Wang, B.; Gu, D.; Wang, S.; Qiao, Y.; et al. Synthesis of diboronic acid-based fluorescent probes for the sensitive detection of glucose in aqueous media and biological matrices. *ACS Sens.* **2021**, *6*, 1543–1551. [CrossRef]

26. Wang, C.; Li, Y.; Wei, Y. A sandwich boronate affinity sorbent assay for glucose detection facilitated by boronic acid-terminated fluorescent polymers. *Sens. Actuators B Chem.* **2017**, *247*, 595–601. [CrossRef]

27. Rastede, E.E.; Tanha, M.; Yaron, D.; Watkins, S.C.; Waggoner, A.S.; Armitage, B.A. Spectral fine tuning of cyanine dyes: Electron donor—acceptor substituted analogues of thiazole orange. *Photochem. Photobiol. Sci.* **2015**, *14*, 1703–1712. [CrossRef]

28. Anderson, J.M. Biological responses to materials. *Annu. Rev. Mater. Sci.* **2001**, *31*, 81–110. [CrossRef]

29. Sutherland, K.; Mahoney, J.R.; Coury, A.J.; Eaton, J.W. Degradation of biomaterials by phagocyte-derived oxidants. *J. Clin. Investig.* **1993**, *92*, 2360–2367. [CrossRef]

30. Anderson, J.M.; Rodriguez, A.; Chang, D.T. Foreign body reaction to biomaterials. *Semin. Immunol.* **2008**, *20*, 86–100. [CrossRef]

31. Larkin, J.D.; Frimat, K.A.; Fyles, T.M.; Flower, S.E.; James, T.D. Boronic acid based photoinduced electron transfer (PET) fluorescence sensors for Saccharides. *New J. Chem.* **2010**, *34*, 2922–2931. [CrossRef]

32. Zwinkels, J.C.; DeRose, P.C.; Leland, J.E. Chapter 7—Spectral Fluorescence Measurements. In *Experimental Methods in the Physical Sciences*; Germer, T.A., Zwinkels, J.C., Tsai, B.K., Eds.; Academic Press: Cambridge, MA, USA, 2014; Volume 46, pp. 221–290.